Down-Regulation of Osteopontin Suppresses Growth and Metastasis of Hepatocellular Carcinoma Via Induction of Apoptosis

JIAN ZHAO,[*,‡] LI DONG,[*,§,‖] BIN LU,[*] GUOBIN WU,[*,¶] DONGMEI XU,[§] JINGJING CHEN,[*] KAI LI,[*] XIN TONG,[*] JIANXIN DAI,[*,‡] SIDE YAO,[§] MENGCHAO WU,[*] and YAJUN GUO[*,‡]

International Cancer Institute and Eastern Hospital of Hepatobiliary Surgery, Second Military Medical University, Shanghai, People's Republic of China; ‡E-Institute of Universities, Immunology Division and Shanghai Center for Cell Engineering and Antibody, Shanghai, People's Republic of China; §Shanghai Institute of Applied Physics, China Academy of Sciences, Shanghai, People's Republic of China; ‖Graduated School of Chinese Academy of Science, Beijing, People's Republic of China; and the ¶Guangxi Cancer Hospital, Guangxi Medical University, Guangxi, People's Republic of China

Background & Aims: **Expression of osteopontin correlates with tumor progression and metastasis. The mechanisms by which osteopontin promotes tumor cell survival remain unclear. Here we used short-hairpin RNA–mediated gene silencing to investigate the antitumor effects by osteopontin depletion in hepatocellular carcinoma (HCC).** ***Methods:*** **We applied polyethylenimine nanoparticles to deliver a short-hairpin RNA for depletion of osteopontin expression in HCC cells. Tumorigenicity and metastatic potentials of HCC cells were studied in vitro and in nude mice. Nuclear factor-κB (NF-κB) activation was analyzed by gel shift assay and luciferase analysis. The expressions of integrins were examined by real-time reverse-transcription polymerase chain reaction. Apoptosis was examined by terminal deoxynucleotidyl transferase–mediated deoxyuridine triphosphate nick-end labeling assay and mitochondrial membrane potential analysis.** ***Results:*** **Down-regulation of osteopontin inhibited HCC cell growth, anchorage-independent growth, adhesion with fibronectin and invasion through extracellular matrix in vitro, and suppressed tumorigenicity and lung metastasis in nude mice. Osteopontin silencing resulted in suppression of αv, β1, and β3 integrin expressions, blockade of NF-κB activation, inhibition of Bcl-2/Bcl-xL and XIAP expressions, increase of Bax expression, and induction of a mitochondria-mediated apoptosis. Furthermore, down-regulation of osteopontin inhibited drug-induced NF-κB activation and sensitized HCC cells to chemotherapeutic agents in vitro, which led to complete regression of HCC xenografts in nude mice.** ***Conclusions:*** **Osteopontin may facilitate tumorigenesis and metastasis through prevention of tumor cells from apoptosis. RNA interference–mediated depletion of osteopontin may be a promising strategy for the treatment of HCC by sensitizing the chemotherapeutic drugs.**

Recent evidence has shown that the expression of osteopontin (OPN) is increased significantly in hepatocellular carcinoma (HCC), which associates closely with poor prognosis, early recurrence, tumor aggressiveness, and metastasis.[1,2] OPN, an extracellular matrix protein, binds to $\alpha_v\beta$ integrins and CD44 family of receptors to propagate cellular signals on extracellular matrix (ECM) degradation, angiogenesis, and tumor cell apoptosis.[3–5] The mechanisms by which OPN promotes tumor cell survival are still unclear. Soluble OPN inhibits growth factors and cytokine depletion induced apoptosis in adherent endothelial cells, which involves enhanced Bcl-xL expression.[6] OPN contributes to antiapoptotic signaling of melanocytes in dermal collagen through interaction with integrin $\alpha_v\beta_3$.[7] OPN-deficient cardiac fibroblasts undergo increased cell death in response to hydrogen peroxide through a caspase-3–independent pathway.[8] OPN null mice show a significant delay in 7,12-dimethylbenzanthracene–induced papilloma development as a result of enhanced apoptotic effects.[9] OPN treatment confers colon cancer and gastric cancer cells an increased resistance to ultraviolet-induced apoptosis via integrin activation.[10]

Efforts have been made to inhibit tumor progression and metastasis by targeting OPN. [4] Suppression of OPN by antisense oligonucleotides or RNA-mediated interference and inhibition of OPN protein by antibodies or synthetic peptides have been used as the tools for cancer therapy.[4] OPN-neutralizing antibody efficiently blocked invasion and metastasis of HCC cells both in vitro and in vivo.[2] Blockade of OPN expression using small interfering RNA effectively suppressed metastasis of CT26 murine colon adenocarcinoma and human esophageal squamous cell carcinoma.[11,12]

Polymeric nanoparticles for gene delivery have drawn much attention for its resistance to nuclease degradation

Abbreviations used in this paper: 5-FU, 5-fluorouracil; GFP, green fluorescent protein; MMP, mitochondrial membrane potential; NF-κB, nuclear factor-κB; OPN, osteopontin; shNon, nonsilencing shRNA; shOPN, shRNA targeting OPN; shRNA, short-hairpin RNA; TMRE, tetramethylrhodamine ethylester; TUNEL, terminal deoxynucleotidyl transferase–mediated deoxyuridine triphosphate nick-end labeling.

0016-5085/08/$34.00
doi:10.1053/j.gastro.2008.05.025

and sustained duration of plasmid DNA administration.[13,14] In this study, we applied spheric polyethylenimine nanoparticles (named *M-PEI*) of 80 nm prepared by photo-Fenton reaction in aqueous solution[15,16] to deliver a short-hairpin RNA (shRNA) targeting osteopontin and investigated the therapeutic efficacy of this novel approach in the treatment of human HCC in a xenografted mouse model system.

Materials and Methods

Construction of shRNA Plasmid Vectors

The sequence targeting human OPN for RNA interference was 5′ GGACAGTTATGAAACGAGT 3′. Sequence (5′ TTCTCCGAACGTGTCACGT 3′) targeting none of the known genes was used for negative control. Oligonucleotides of shRNA including a TTCAAGAGA loop motif were synthesized and inserted into pGCsi vector containing H1 promoter, T6 terminal sequences, and green fluorescent protein (GFP) reporter gene with a standard cloning procedure by GeneChem (Shanghai, China).

Cell Cultures and Transfection

Cells were grown in Dulbecco's modified Eagle medium supplemented with 10% fetal bovine serum in a humidified incubator at 37°C in a 5% CO_2 atmosphere. Transfection of plasmids was performed using M-PEI in 6-well tissue culture plates as described previously.[15] Briefly, 3.6 μg plasmid was dissolved in 100 μL 0.9% NaCl, 14.4 μg of M-PEI then was pipetted to plasmid. The plasmid/M-PEI mixture then was added to cells in serum-free Dulbecco's modified Eagle medium. IκBα kinase β mammalian–expressing plasmids were from GeneCopoeia (Guangzhou, China).

Anchorage-Independent Growth Assay

For anchorage-independent growth assays, cells were seeded in 0.3% agarose over a 0.6% agarose bottom layer at a density of 500 cells per well in a 24-well plate. After 3 weeks, the numbers of colonies greater than 100 μm in diameter were counted.

Cell Invasion and Adhesion Assay

Invasion of cells through the ECM was determined by the Cell Invasion Assay Kit (Chemicon, Temecula, CA). The number of cells invading through the ECM was counted by 5 randomly selected visual fields, and the extent of invasion was expressed as the average number of cells per microscopic field at a magnification of 200. Ninety-six–well plates coated with 10 μg/mL fibronectin (Calbiochem, San Diego, CA) were used for adhesion assay as described previously.[17]

Apoptosis Analysis

The fluorescein FragEL DNA Fragmentation Detection Kit (Calbiochem) was used for the terminal deoxynucleotidyl transferase–mediated deoxyuridine triphosphate nick-end labeling (TUNEL) assay. The fluorescein of cells carrying DNA labeled with fluorescein isothiocyanate–deoxyuridine triphosphate (TUNEL-positive cells) was analyzed by Becton Dickinson (Franklin Lakes, NJ) FACscan.

For in vivo apoptosis assay, the formalin-fixed paraffin sections were deparaffinized and incubated with TUNEL reaction mixture. Apoptotic cells were observed under a fluorescence microscope (Olympus, Tokyo, Japan).

Measurement of Mitochondrial Membrane Potential

Cells were incubated with tetramethylrhodamine ethylester (TMRE) by the MitoShift Kit (Trevigen, Gaithersburg, MD) and observed under a fluorescence microscope. In healthy cells, the TMRE dye accumulates in the mitochondria and appears bright red by fluorescence microscopy, but in apoptotic cells the mitochondrial membrane potential collapses and the TMRE dye cannot accumulate within the mitochondria.

Reverse-Transcription Polymerase Chain Reaction Analysis

Total RNA was isolated using the RNeasy mini kit (Qiagen, Hilden, Germany), and genomic DNA was removed using the RNase-Free DNase set (Promega, Madison, WI). First-strand cDNA was generated using the Reverse Transcription System kit (Promega). For quantification of integrin and CD44 messenger RNA expression, real-time polymerase chain reaction was performed as described previously.[18]

Subcellular Fractionation and Western Blotting Analysis

Cytosol and mitochondria fractionation was performed by the centrifugation technique as described previously.[19] Nuclear extracts were made using NE-PER Nuclear and Cytoplasmic Extraction Reagents (Pierce Biotechnology, Rockford, IL). Total cell lysate was prepared in 1 × sodium dodecyl sulfate buffer. Proteins at the same amount were separated by sodium dodecyl sulfate–polyacrylamide gel electrophoresis and transferred onto polyvinylidene difluoride membranes. After probing with individual antibodies, the antigen–antibody complex was visualized by the enhanced chemiluminescence reagent Supersignal (Pierce Biotechnology). The antibodies used were anti–caspase-3, anti–caspase-9, anti-X-linked inhibitor of apoptosis protein (XIAP), anti-poly (ADP-ribose) polymerase (PARP), anti–cytochrome *c*, and anti-OPN (R&D Systems, Minneapolis, MN), anti–Bcl-2, anti–Bcl-xL, and anti-Bax (Santa Cruz Biotechnology, Santa Cruz, CA), anti-p-Akt, anti–nuclear factor κB (NF-κB) p65, and anti-IκBα (Boster Biotechnology, Wuhan, China), anti-GFP and anti-human matrix matallopeptidase 2 (MMP2; Beyotime, Haimen, China).

OPN Enzyme-Linked Immunosorbent Assay

Cells were deprived of serum 24 hours after transfection. The conditioned media was collected and viable cell numbers were assessed by trypan-blue staining every 12 hours. OPN concentrations in conditioned media were measured using a quantitative immunoassay enzyme-linked immunosorbent assay kit (QuantiKine Assay; R&D Systems). OPN levels were normalized to viable cell numbers and calculated according to the following formula: OPN levels (ng/mL) = OPN concentrations in conditioned media (ng/mL) × (cell numbers in mock wells/cell numbers in shRNA-transfected wells). Triplicate samples were analyzed.

Electrophoretic Mobility Shift Assay

Electrophoretic mobility shift assay was performed using the LightShift chemiluminescent electrophoretic mobility shift assay kit (Pierce Biotechnology). Double-stranded gel shift probes corresponding to the human consensus NF-κB sequences[20] (5′-AGTTGAGGGGACTTTCCCAGGC-3′) were end-labeled with biotin.

Luciferase Reporter Assays

Cells were transfected with NF-κB–driven luciferase plasmid together with the pRL-TK, which contains the herpes simplex virus thymidine kinase (HSK-TK) promoter to provide low to moderate levels of *Renilla* luciferase expression, vector as a control for transfection efficiency using Lipofectamine 2000 (Invitrogen, Carlsbad, CA). The luciferase activities were measured using the Dual Luciferase Reporter Assay System (Promega).

Gelatin Zymography

MMP-2 activity was detected by zymography as described previously.[21] Briefly, the conditioned medium and tumor lysates were collected and the equal amounts of protein were separated by 10% sodium dodecyl sulfate–polyacrylamide gel electrophoresis containing 0.1% gelatin without reducing agent. The gels were washed with 2.5% Triton X-100 and incubated in 20 mmol/L glycine, 10 mmol/L $CaCl_2$, and 1 mmol/L $ZnCl_2$ (pH 8.3) at 37°C for 24 hours to allow the gelatinases to digest the gelatin structure. The gels were stained with Coomassie Blue and destained to visualize the results.

Tumorigenicity Assay

Six-week-old male BALB/c nude mice were purchased from the Shanghai Experimental Animal Center of Chinese Academy of Sciences (Shanghai, China). All mice were maintained under pathogen-free conditions in laminar flow boxes in accordance with established institutional guidance and approved protocols. Two days after transfection with shRNA plasmids, 5×10^6 HCC-LM3 cells were injected subcutaneously into the right flanks of nude mice. The tumor volume was calculated according to the following formula: V = length × width^2 × 0.5. Animals were killed for histopathology examination at day 35 after cell inoculation.

Treatment of Mice With HCC Xenografts

For in vivo treatment experiments, mice inoculated with 5×10^6 HCC-LM3 cells were divided randomly into 6 groups (6 mice/group) when tumor volume reached 100 mm^3. Mice were treated daily for 5 days by intratumoral injection of 20 μg shRNA plasmids mixed with 80 μg M-PEI. One day after injection, the mice were dosed intraperitoneally with or without 5-fluorouracil (5-FU) at a concentration of 10 mg/kg body weight daily for 5 days. Tumor volume was monitored.

Statistical Analysis

Statistical analysis was performed using the Analysis ToolPack provided by Microsoft Excel (Beijing, China). A 2-sample Student *t* test, assuming unequal variances, was used to determine the equality of the means of 2 samples. Results were considered statistically significant at a *P* value of less than .05.

Results

M-PEI–Mediated shRNA Delivery Inhibits OPN Expression in HCC Cells

About 50%–60% of cells were transfected with shRNA plasmids by M-PEI, as monitored by GFP expression in HCC cells (Figure 1*A*). Transfection with shRNA targeting OPN (shOPN), but not nonsilencing shRNA (shNon), reduced OPN expression by about 50% as detected by reverse-transcription polymerase chain reaction and Western blotting analyses compared with mock controls (Figure 1*B* and *C*). Expression of GFP and inhibition of OPN expression lasted up to 14 days posttransfection (Figure 1*D*), which might be owing to plasma DNA entrapped in PEI polymeric particles showing a sustained release pattern.[13,15] The secreted OPN in the culture medium was reduced significantly in shOPN-transfected HCC-LM3 cells (Figure 1*E*). Thus, M-PEI–mediated shOPN transfection efficiently inhibits OPN expression in HCC cells.

Inhibition of Cell Growth and Metastatic Potential of HCC Cells by OPN Depletion In Vitro

shOPN, but not shNon, significantly inhibited the growth and anchorage-independent growth of HCC cells (Figure 2*A* and *B*). Addition of recombinant human OPN generated from mouse myeloma cell NSO (rhOPN; R&D Systems) or HCC-LM3 conditioned media could not reverse the inhibitory effect of shOPN on cell growth (Figure 2*A*). A marked reduction of adhesion and invasion abilities was observed in shOPN-transfected cells, which could be reversed by addition of rhOPN (Figure 2*C* and *D*). Moreover, shOPN-transfected HCC-LM3 cells showed a drastic reduction of MMP-2 expression (Figure 2*E*). Thus,

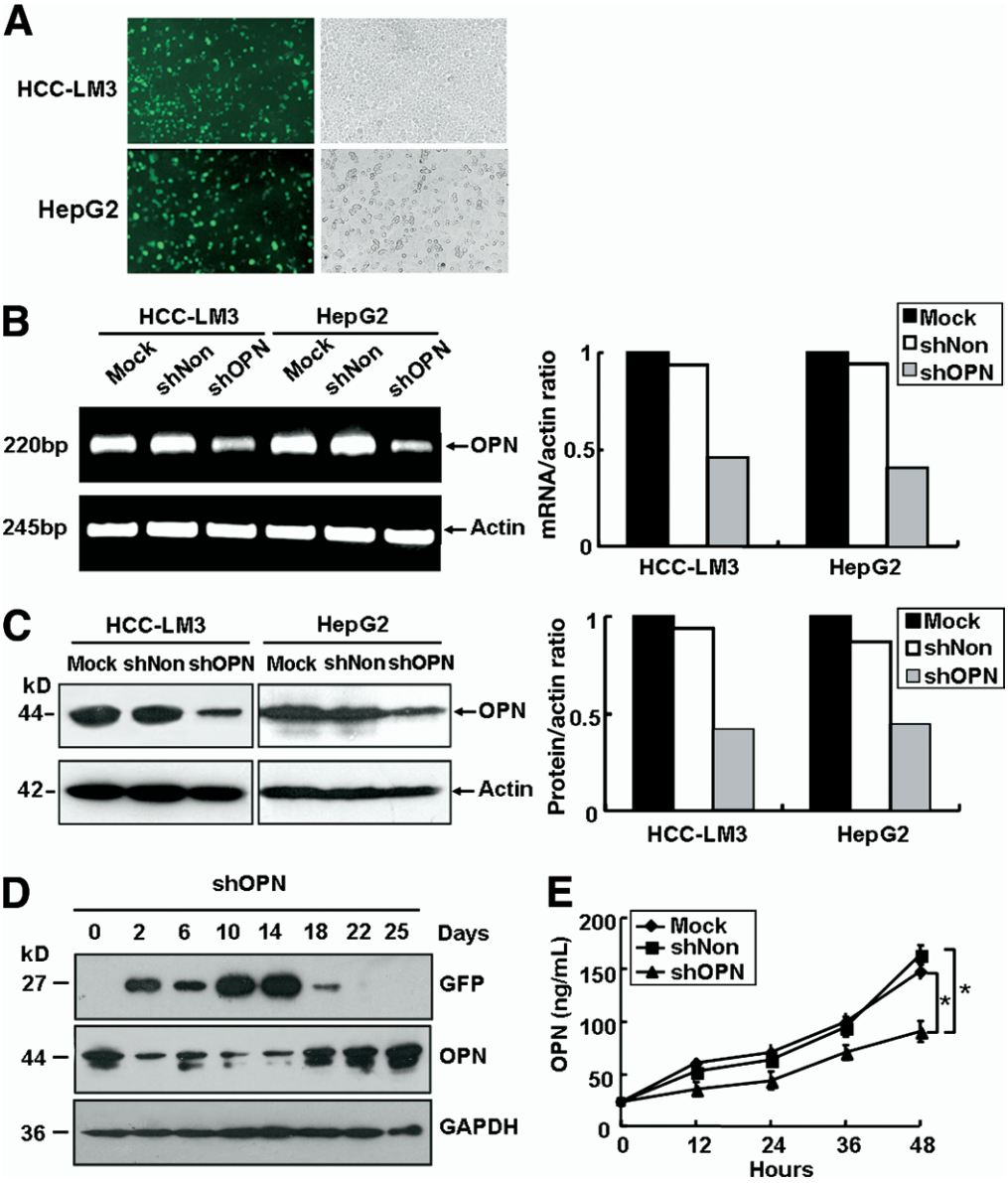

Figure 1. M-PEI–mediated shRNA plasmid delivery inhibited OPN expression in HCC cells. (*A*) HCC cells were transfected with shNon by M-PEI. The efficiency of transfection was monitored by detecting GFP expression under fluorescence microscopy at 48 hours posttransfection. Phase-contrast images of cells are shown in the corresponding right-hand column (magnification, 100×). (*B* and *C*) At 48 hours posttransfection, RNA and total proteins were extracted and subjected to (*B*) reverse-transcription polymerase chain reaction analysis or (*C*) Western blotting for OPN expression. OPN expression was quantified by densitometric analysis of the OPN bands normalized to the actin bands. (*D*) Analyses of GFP and OPN protein expressions in HCC-LM3 cells at various times after transfection with shOPN. (*E*) Levels of the secreted OPN in the serum-free media were evaluated by enzyme-linked immunosorbent assay. Data are shown as the means ± SD from triplicate experiments. (*$P < .05$). GAPDH, glyceraldehyde-3-phosphate dehydrogenase.

depletion of OPN has an inhibitory effect on the growth and invasion of HCC cells.

OPN Depletion Suppresses Tumorigenesis and Lung Metastasis in HCC Xenografted Mice

Eight days after tumor cell inoculation, all mice injected with shNon-transfected or mock-treated HCC-LM3 cells developed tumors in nude mice. However, it took 13 to 28 days for shOPN-transfected cells to develop tumors (Figure 3*A*). Growth of shOPN-modified HCC-LM3 cells was suppressed significantly compared with that of shNon-transfected or mock-treated cells (Figure 3*B*). The tumor volumes and weights of shOPN-modified HCC-LM3 xenografts were only about 20% and 25% of that of mock-treated xenografts 35 days after implantation (Table 1). Furthermore, the incidence of lung metastasis dropped to zero in shOPN-modified HCC-LM3 xenografted mice, which is significantly different from that in the mock-treated group (83.3%) or the shNon-modified group (71.4%) (Figure 3*C*, Table 1). Inhibition of OPN expression was confirmed by detection of OPN levels in plasma (Figure 3*D*),

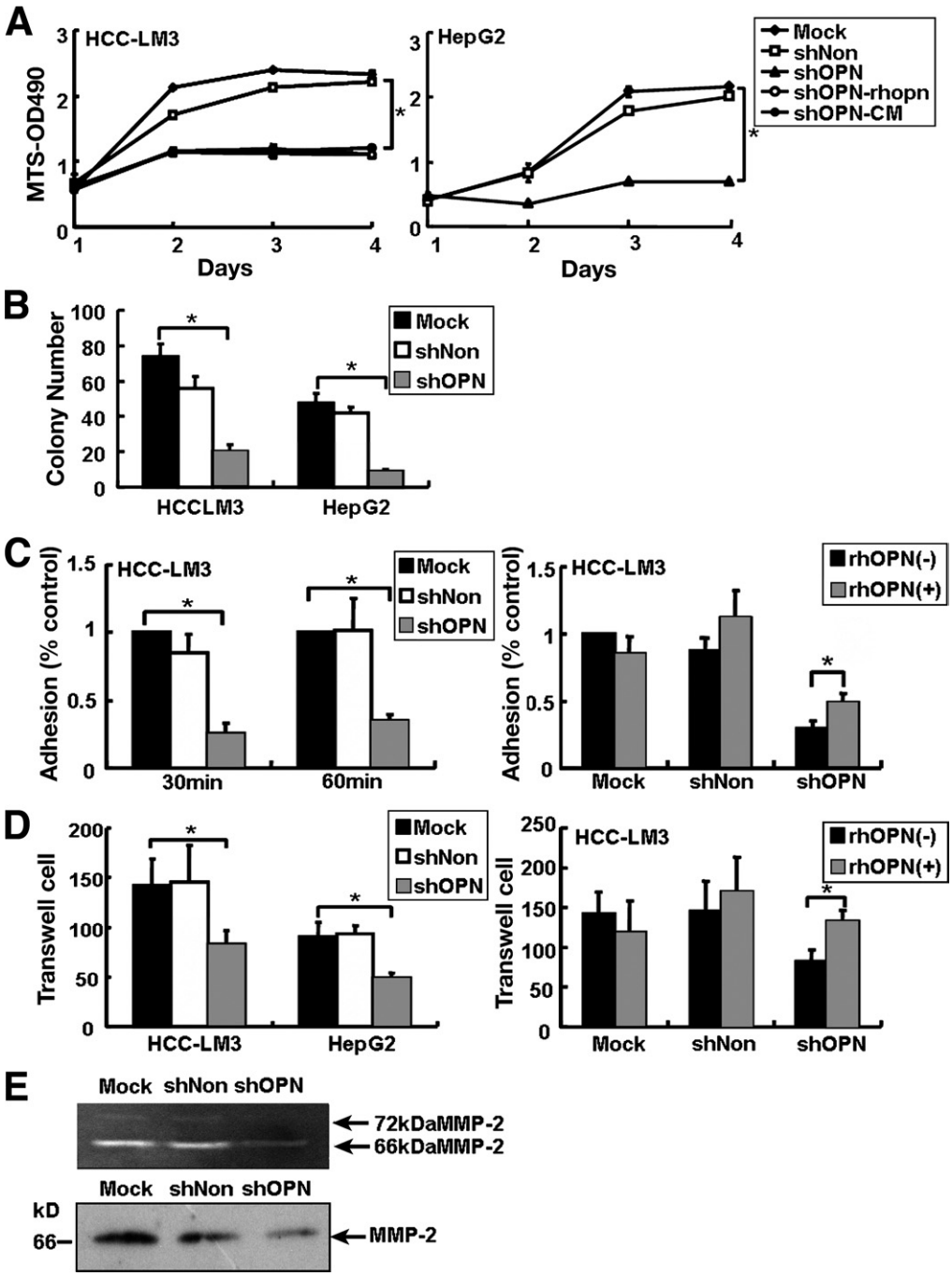

Figure 2. Down-regulation of OPN inhibited cell growth and metastatic potentials in HCC cells in vitro. (*A*) At 24 hours posttransfection, HCC cells were seeded in 96-well plates with or without rhOPN (5 μg/mL) or HCC-LM3 conditioned medium (CM) for MTS assay (Promega). Values were given as the means ± SD of 6 wells. (*$P < .05$). (*B*) HCC cells were seeded in semisolid soft agar medium to monitor anchorage-independent growth. The numbers represented the mean number of colonies of 3 independent experiments ± SD (*$P < .05$). (*C*) HCC-LM3 cells were plated in 96-well plates precoated with fibronectin and allowed to adhere for 30 or 60 minutes. Alternatively, the cells were incubated with or without rhOPN (5 μg/mL) for 2 hours before being plated in 96-well plates and allowed to adhere for 30 minutes. Relative cell adhesion was calculated by MTT assay with comparison with mock-treated cells. Mean values ± SD of 3 independent experiments were shown (*$P < .05$). (*D*) HCC cells were incubated with ECM in the presence or absence of rhOPN (5 μg/mL) for 72 hours. Invading cell numbers are the average count of 5 random microscopic fields. Values shown are means ± SD (*$P < .05$). (*E*) HCC-LM3 cells were serum-deprived for 24 hours. The supernatants were collected and MMP-2 activity was analyzed by zymography and Western blotting. Equal amounts of total proteins were used in each lane. MTS, (3-(4,5-Dimethylthiazol-2-yl)-5-(3-carboxymethoxyphenyl)-2-(4-sulfophenyl)-2H-tetrazoloium, inner salt); MTT, (3-(4-,5-Dimethylthiazol-2-yl)-2,5-diphenyltetrazoliumbromide, a tetrazole).

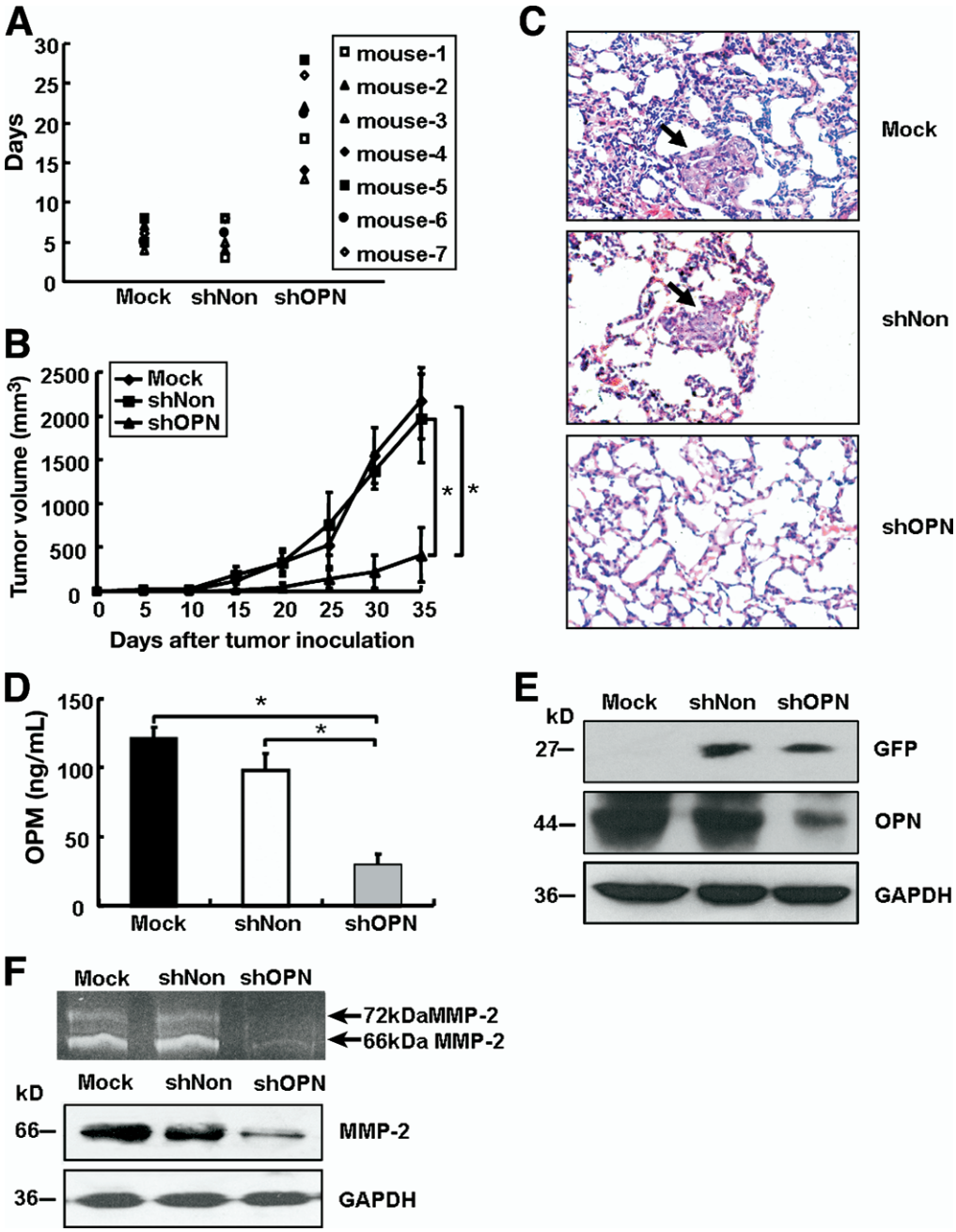

Figure 3. Down-regulation of OPN inhibited tumorigenicity and metastasis of HCC xenografts in nude mice. (*A*) Tumor formation time of each mouse was monitored. (*B*) The tumor volume of each group was scored every 5 days. Data represent the means ± SD (*$P < .05$). (*C*) Representative lung tissue sections (H&E stain: magnification, 400×) from each group at day 35 after cell inoculation. Arrows indicate metastatic tumors. (*D*) Comparison of the mean plasma OPN levels by enzyme-linked immunosorbent assay in each group at day 35. Data represent the means ± SD (*$P < .05$). (*E*) Total proteins were extracted from tumor tissues derived from each group 35 days after implantation and subjected to Western blotting with anti-OPN and anti-GFP antibodies. (*F*) The tumor samples in each group at day 35 were lysed by homogenization in phosphate-buffered saline and MMP-2 activity was analyzed by gelatin zymography and Western blotting. Equal amounts of total proteins were used in each lane. GAPDH, glyceraldehyde-3-phosphate dehydrogenase.

as well as detection of OPN and GFP expression by Western blotting in tumor samples 35 days after implantation (Figure 3*E*). Inhibition of MMP2 expression by shOPN was observed in tumor lysates (Figure 3*F*). These data suggest that OPN-depletion leads to significant inhibition of tumorigenesis and metastasis of HCC in vivo.

OPN Silencing Induces Mitochondria-Mediated Apoptosis

After transfection with shOPN, most HCC cells had shrunk and detached from the plate under serum starvation. In contrast, the shNon-transfected cells remained attached to the dish and showed normal mor-

Table 1. Osteopontin shRNA Inhibits Tumorigenesis and Metastasis of HCC-LM3 Cells in Nude Mice

	Tumor size		Lung metastasis	
Treatment groups	Volume, mm^3	Weight, g	Cases (%)	Metastasis, no.
Mock	2167 ± 428	2.37 ± 0.23	5 of 6 (83.3%)	5.2 ± 1.3
shNon	1971 ± 500	2.12 ± 0.34	5 of 7 (71.4%)	4.4 ± 2.3
shOPN	416 ± 314*	0.605 ± 0.27*	0 of 7 (0)*	0*

NOTE. Evaluation of lung metastasis in mice was performed on day 35 after subcutaneous implantation of HCC-LM3 cells. Tumor sizes are presented by both volume in cubic millimeters and weight in grams (mean ± SD). Lung metastasis is denoted as both the positive metastases in the lungs (the percentages are indicated in parentheses) and the average number of metastases (no.) in lungs per positive case (mean ± SD). *$P < .05$, compared to mock treatment.

phology (Figure 4*A*). The cell death in the shOPN-treated group was significantly higher than that in the shNon or mock-treated groups, which was strongly enhanced by serum starvation in HCC cells (Figure 4*B*). Addition of rhOPN could reverse anti-OPN antibody-induced but not shOPN-induced cell death (Figure 4*C*).The percentage of TUNEL-positive apoptotic cells greatly increased by OPN depletion compared with shNon-transfection, which was greatly enhanced by serum starvation (Figure 4*D*). Another shOPN construct targeting 5'-GCATTCCGATGTGATTGAT-3' resulted in similar effects (Figure 4*E*). Addition of rhOPN could not reverse shOPN-induced apoptosis (Figure 4*E*).

Apoptosis was examined further by in situ TUNEL assay on HCC-LM3 xenografted tumor tissues. The apoptotic nuclei, seen as green color excited under fluorescence microscope, were greatly increased in shOPN-transfected HCC-LM3 xenografts (Figure 4*F*). The percentage of apoptotic cells in the shOPN group was 2 or 3 times higher than that in the shNon or mock groups.

Procaspase-3 and -9 were greatly decreased at 48 hours posttransfection with shOPN (Figure 5*A*). PARP, the substrate of caspase-3, was found cleaved with an 85-kilodalton fragment after shOPN transfection (Figure 5*A*). Furthermore, the broad-spectrum caspases inhibitor N-tert-butoxy-carbonyl-Val-Ala-Asp-fluoromethylketone significantly inhibited shOPN-induced cell death (Figure 5*B*). Thus, shOPN induced apoptosis is caspase-dependent in HCC cells.

Transfection with shOPN resulted in a significant loss of mitochondrial membrane potential indicated by a substantial reduction of TMRE staining (Figure 5*C*), as compared with surrounding nontransfected cells. Down-regulation of OPN caused a dramatic accumulation of Bax and obvious elimination of Bcl-2 at mitochondria, as well as release of cyto-*c* from mitochondria to cytosol (Figure 5*D*). OPN silencing resulted in an obvious decrease of Bcl-xL, Bcl-2, and XIAP, and a dramatic increase of Bax expression, which could not be reversed by addition of rhOPN (Figure 5*E*). However, IκBα kinase β, which activates NF-κB through phosphorylation and degradation of IκBα, blocked shOPN-induced decrease of Bcl-2 and induction of Bax (Figure 5*F*), indicating that the alterations of Bcl-2 and Bax expression might be the result of inhibition of NF-κB activity by OPN depletion. Thus, OPN depletion might induce mitochondria-mediated apoptosis through regulation of the expression of Bcl-2 and IAPs family members.

OPN Depletion Inhibits αv, β1, and β3 Integrin Expression and Blocks NF-κB Activity

Expressions of integrin αv, β1, and β3, and CD44 were much higher in HCC-LM3 cells than HL7702 cells (Figure 6*A*). OPN depletion greatly decreased the expressions of αv, β1, and β3 integrin in HCC-LM3 cells (Figure 6*A*). Addition of rhOPN attenuated anti-OPN antibody–induced but not shOPN-induced αv, β3 integrin suppression (Figure 6*A*). However, the mechanism for down-regulation of the expressions of integrins by OPN depletion still need to be investigated further.

OPN could activate both Akt and NF-κB activities on interaction with αv β1 and αvβ3 integrins to promote cell survival and motility.[5] We first measured the activity of Akt by assessing phosphorylation of Akt after OPN depletion. Phosphorylation of Akt was not affected by OPN knockdown (Figure 6*B*). However, OPN depletion greatly inhibited the amount of p65 subunit of NF-κB and prevented the nuclear accumulation of p65 induced by serum starvation or 5-FU stimulation (Figure 6*B*). NF-κB transcriptional activity was greatly enhanced in HCC-LM3 cells compared with HL7702 cells (Figure 6*C*). Down-regulation of OPN significantly inhibited NF-κB activity and cisplatin-induced NF-κB activation in HCC-LM3 cells (Figure 6*C*). NF-κB DNA-binding activities induced by serum starvation or cisplatin and 5-FU treatment also were strongly attenuated by OPN depletion, which could not be reversed by addition of rhOPN (Figure 6*D*). Next, the expression of NF-κB inhibitor IκBα was determined by Western blotting. Treatment of cisplatin caused a decrease of IκBα within 30 minutes and then the amount of IκBα returned to basal levels after 60 minutes because of its NF-κB–dependent do novo synthesis. OPN depletion greatly enhanced the amount of IκBα and completely blocked cisplatin-induced turnover of IκBα (Figure 6*E*). These data suggest that depletion of OPN might block chemotherapy drug–induced NF-κB activation.

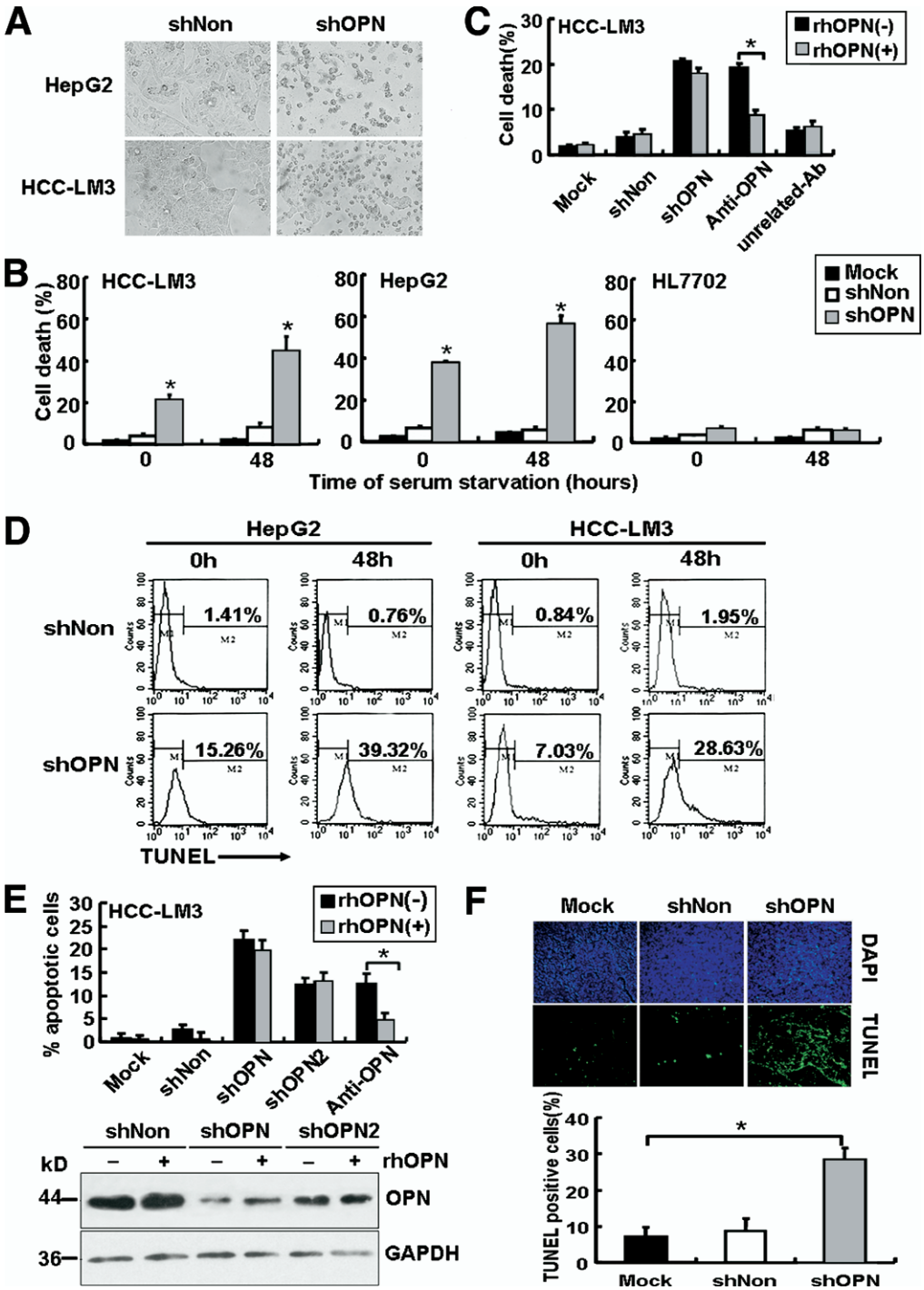

Figure 4. Down-regulation of OPN-induced apoptosis in HCC cells. HCC cells were transfected with shRNA plasmids for 24 hours, and then exposed to serum starvation for 48 hours. (*A*) Photomicrographs showed morphologic changes in HCC cells (magnification, 200×). (*B*) Cell death was monitored by trypan blue staining and expressed as the percentage of blue dead cells relative to the total cell number. Data were presented as means ± SD from 3 independent experiments (*$P < .05$). (*C*) shRNA-transfected and anti-OPN antibody (2 μg/mL; R&D Systems)–treated cells were incubated with or without rhOPN (5 μg/mL) for 48 hours and the cell death was determined as in *B* (*$P < .05$). (*D*) Apoptotic cells were detected by fluorescence flow cytometry with TUNEL assay. Numbers above bracketed lines indicate the percentage of TUNEL-positive cells. The experiments were repeated 3 times. (*E*) shRNA-transfected and anti-OPN antibody–treated cells were incubated with or without rhOPN (5 μg/mL) for 48 hours and then cell apoptosis was determined by TUNEL assay (*$P < .05$). Expressions of OPN were confirmed by Western blotting with anti-OPN antibody. (*F*) In situ TUNEL apoptosis analysis was performed in tumor sections derived from the same mice as in Figure 3 at day 35 after cell inoculation. The apoptotic nuclei were seen as green color excited under fluorescence microscopy. Cell nuclei were counterstained with DAPI and seen as blue (magnification, 200×). The percentage of apoptotic cells was calculated by counting green-stained nuclei vs blue-stained nuclei from 6 randomly chosen fields in each section. Data are presented as means ± SD (*$P < .05$). GAPDH, glyceraldehyde-3-phosphate dehydrogenase.

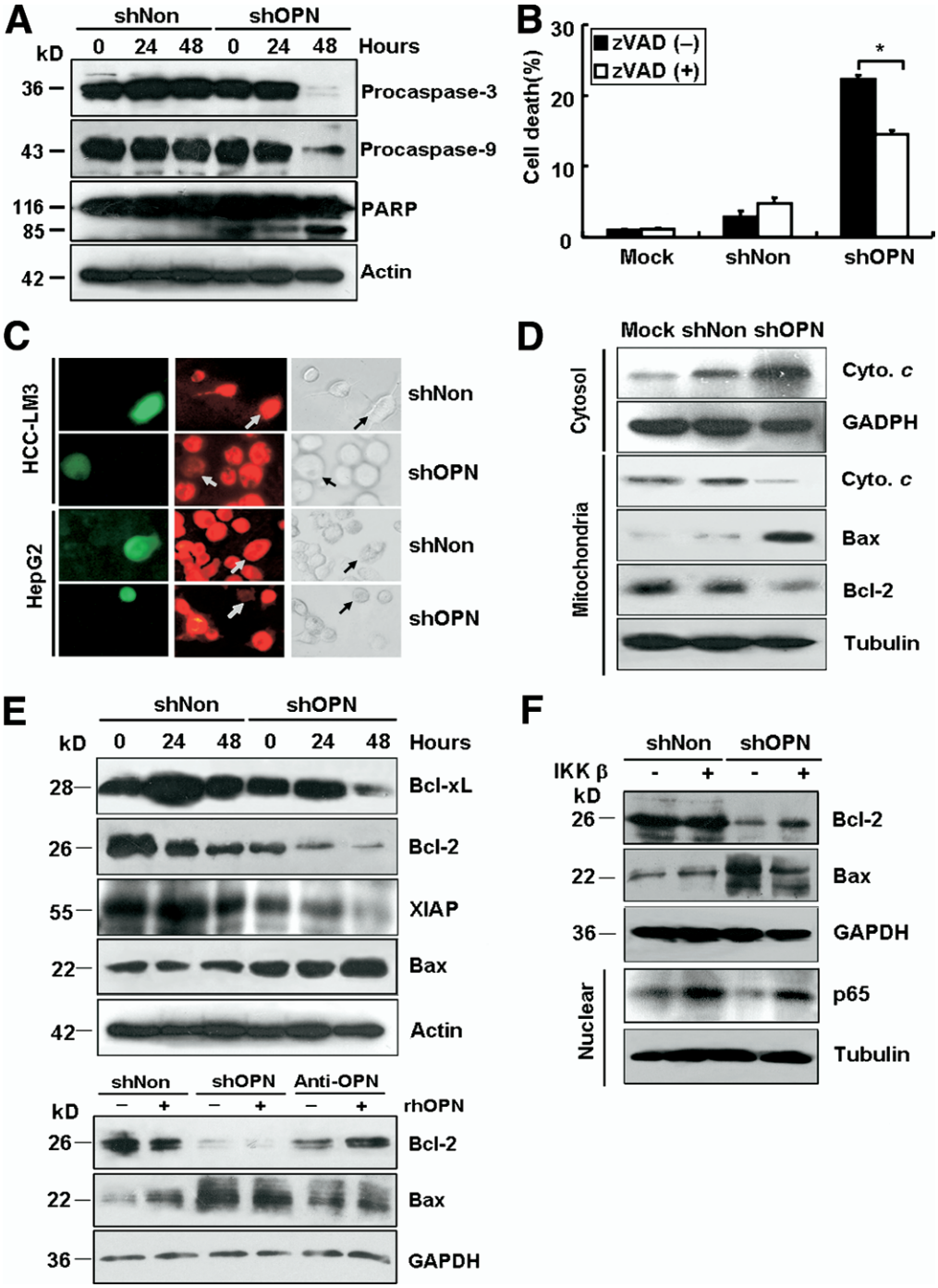

Figure 5. Down-regulation of OPN-induced mitochondria-mediated apoptosis. (*A*) Twenty-four hours after transfection, total proteins were isolated at the various times after serum-starvation and subjected to Western blotting with indicated antibodies. (*B*) Cells were treated with the pan-caspase inhibitor N-tert-butoxy-carbonyl-Val-Ala-Asp-fluoromethylketone (80 μmol/L) 2 hours before being subjected to serum starvation for 48 hours. Cell death was determined by trypan blue staining. Data are presented as means ± SD from 3 independent experiments (*$P < .05$). (*C*) After serum-starvation for 48 hours, mitochondrial potential was determined by TMRE staining. Transfected cells (left panel) with the corresponding TMRE staining profile (middle panel) and phase-contrast images (right panel) were observed under fluorescence microscope (magnification, 400×). Arrows indicate the corresponding transfected cells by TMRE staining or phase-contrast images. (*D*) Cytosolic and mitochondrial subcellular fractions were isolated from the same HCC-LM3 cells as in *C*, and subjected to Western blotting with indicated antibodies. (*E*) shRNA-transfected or anti-OPN antibody–treated HCC-LM3 cells were incubated with or without rhOPN (5 μg/mL) in the serum-free media. Total proteins were subjected to Western blotting with antibodies specific for Bax, Bcl-2, Bcl-xL, and XIAP. (*F*) HCC-LM3 cells were transfected with shRNAs together with or without plasmid encoding IκBα kinase β for 48 hours. Total proteins or nuclear proteins were subjected to Western blotting with indicated antibodies. GAPDH, glyceraldehyde-3-phosphate dehydrogenase.

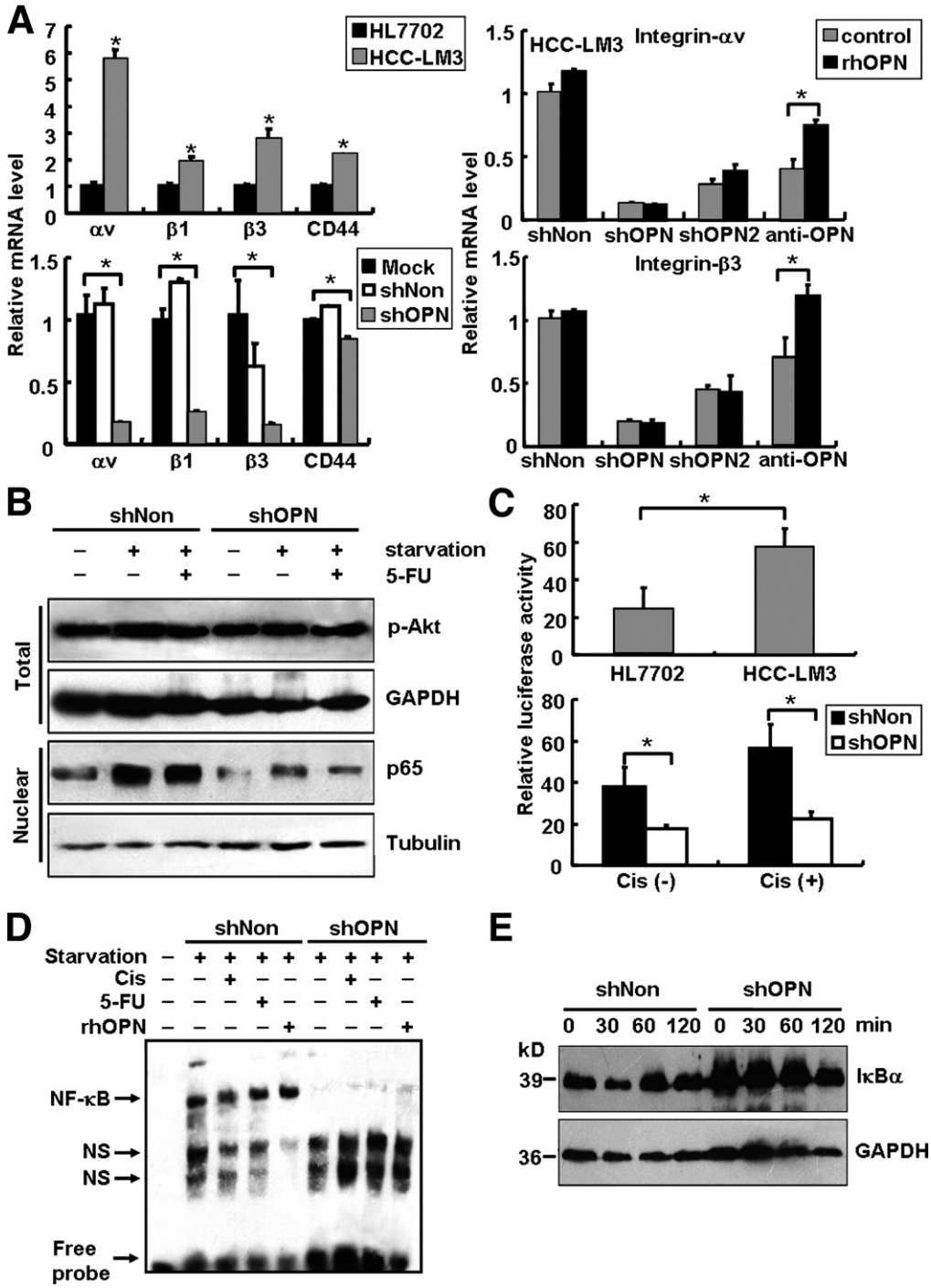

Figure 6. Down-regulation of OPN inhibited integrin expression and suppressed NF-κB activation. (*A*) Real-time reverse-transcription polymerase chain reaction analysis was performed to determine the expressions of integrin αv, $\beta 1$, $\beta 3$, and CD44. Data are presented as means ± SD from 3 independent experiments (*$P < .05$). (*B*) HCC-LM3 cells were subjected to serum-starvation with or without 5-FU (5 μg/mL) treatment. Total proteins or nuclear proteins were isolated 24 hours after treatment and subjected to Western blotting with anti–p-Akt and anti–NF-κB p65 antibodies. (*C*) Cells were transfected with NF-κB–responsive luciferase reporter construct together with or without shRNAs. At 24 hours after transfection, cells were treated with or without cisplatin (0.5 μg/mL). Luciferase activity was determined 24 hours after treatment. Means of triplicate experiments ± SD are shown (*$P < .05$). (*D*) HCC-LM3 cells were exposed to serum starvation with cisplatin (0.5 μg/mL) or 5-FU (5 μg/mL) or rhOPN (5 μg/mL) treatment. Nuclear protein extracts were harvested 24 hours later and subjected to electrophoretic mobility shift assay. Adding no nuclear extract served as negative control in the left-most lane. NS, nonspecific signal. (*E*) HCC-LM3 cells were treated with 0.5 μg/mL cisplatin for the indicated times. Total proteins were isolated and subjected to Western blotting with anti-IκBα antibody. GAPDH, glyceraldehyde-3-phosphate dehydrogenase.

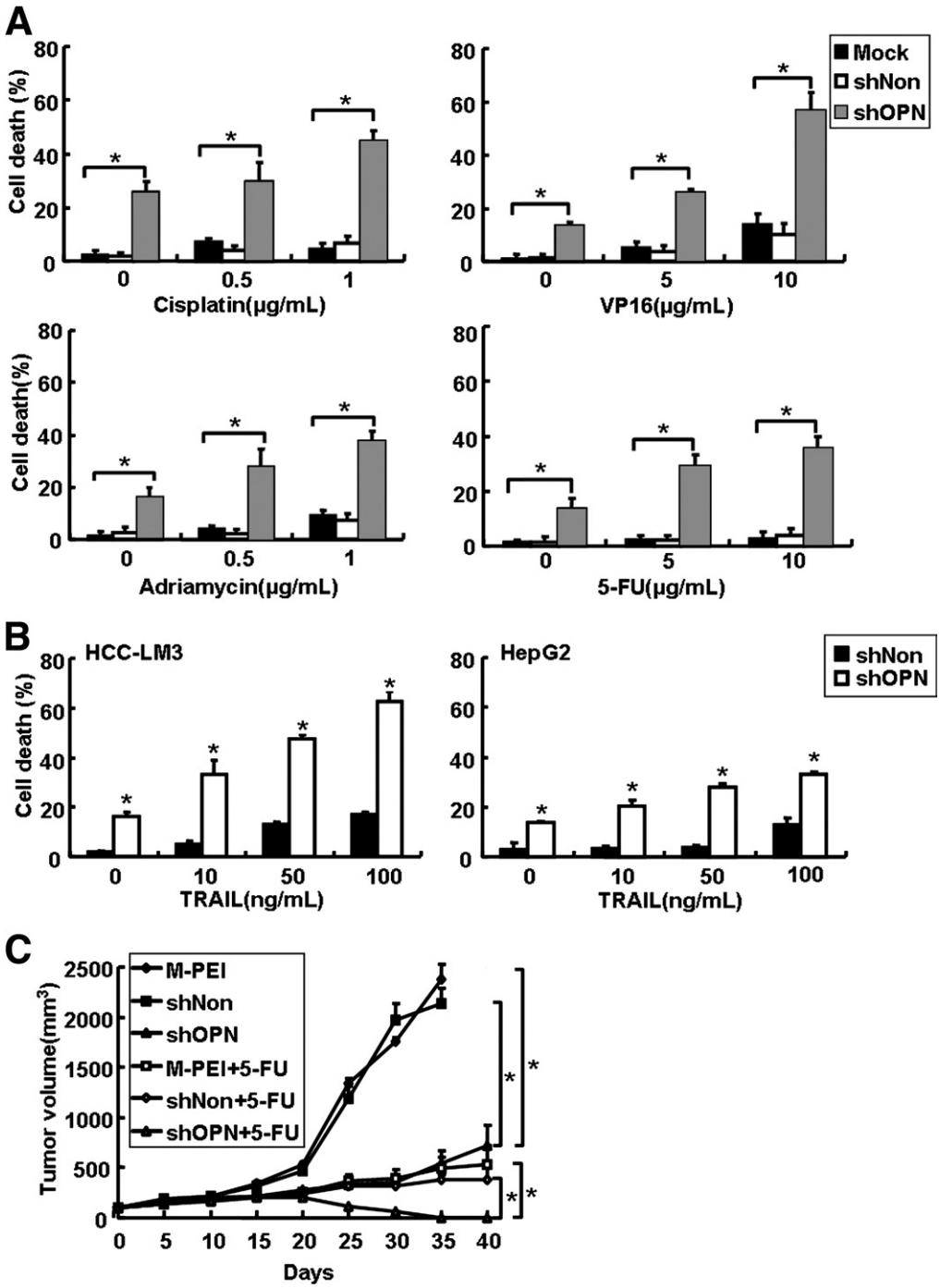

Figure 7. Osteopontin shRNA sensitized HCC cells to chemotherapeutic drugs. (*A* and *B*) shRNA-transfected HCC-LM3 cells were (*A*) incubated with various cytotoxic agents for 24 hours, or (*B*) treated with different concentrations of TRAIL for 48 hours. Cell death was determined by trypan blue staining. Data are presented as means ± SD from 3 independent experiments. (*C*) Tumor volume was measured in HCC-LM3 xenografts receiving different treatments as indicated every 5 days. Data are the means ± SD of the tumor volumes derived from each group (*$P < .05$).

Down-Regulation of OPN Sensitizes HCC Cells to Chemotherapeutic Agents

Depletion of OPN significantly enhanced the sensitivities of HCC-LM3 cells to topoisomerase II inhibitors etoposide and Adriamycin (Merck, San Diego, CA), thymidylate synthase inhibitor 5-FU, as well as the DNA-reactive agent cisplatin, as compared with shNon or mock treatment (Figure 7*A*). TNF-related apoptosis-inducing ligand (TRAIL) induced less than 20% of cell death in HCC-LM3 and HepG2 cells at a dose as high as 100 ng/mL. Down-regulation of OPN dramatically increased TRAIL-mediated cell death (Figure 7*B*). Thus, down-regulation of OPN sen-

sitizes HCC cells to both death receptor and DNA damage–induced cell death.

Intratumoral administration of shOPN significantly inhibited growth of HCC-LM3 xenografts in nude mice compared with treatment with shNon or M-PEI (Figure 7*C*). Notably, intraperitoneal administration of 5-FU in combination with intratumoral administration of shOPN resulted in complete eradication of all 6 HCC-LM3 xenografts (Figure 7*C*). Thus, down-regulation of OPN might be a promising adjuvant for chemotherapy of HCC.

Discussion

Apoptosis plays a central role in tissue homeostasis during both development and adult life. Tumor cells often are deficient in apoptotic regulation, which leads to the expansion of tumor cells, metastasis, and resistance to chemotherapy.[22–24] In the current study, we show that depletion of OPN by RNA-mediated interference promotes HCC cell apoptosis, leading to inhibition of tumorigenesis and metastasis both in vitro and in vivo.

Previous studies have shown that OPN may prevent apoptosis through interaction with integrins and/or CD44 or its variants. OPN-CD44 interaction induced the phosphorylation of Akt in the survival pathway of interleukin-3,[25] whereas OPN-integrin $\alpha v\beta 1$ and $\alpha v\beta 3$ interaction induced endothelial cell survival as a result of the activation of NF-κB.[26] In exploring the molecular mechanism responsible for OPN-depletion–induced apoptosis, a significantly decreased expressions of αv, $\beta 3$, and $\beta 1$ integrin were found. Given that integrins are a large family of cell-surface receptors that bind to ECM components to activate signaling pathways for tumor invasion and metastasis,[27] inhibiting αv, $\beta 3$, and $\beta 1$ integrin expressions and their signaling pathway by OPN depletion might contribute to the inhibitory effect on tumor metastasis and apoptosis. However, how the OPN silencing might inhibit integrin expression still needs to be identified.

Supplement of rhOPN could not reverse shOPN-induced apoptosis in HCC-LM3, which is related directly to the decreased expression of integrins by OPN depletion. The shOPN-treated tumor cells with significantly decreased expression of integrins had a dysfunction to bind and use the secreted or exogenous OPN, which directly contributed to cell apoptosis. However, the importance of intracellular OPN in the regulation of cell survival still needs to be investigated. Because most tumor cells contain high levels of intracellular OPN, the exogenous or tumor cell–secreted OPN might integrate with intracellular OPN to regulate cell survival. Several reports have indicated the vital roles of intracellular OPN. Intracellular OPN is essential for interferon-alfa production by plasmacytoid dendritic cells,[28] and also exists as an integral component of a hyaluronan-CD44-ezrim/radixim/moesin (ERM) attachment complex involved in the migration of embryonic fibroblasts, activated macrophages, and metastatic tumor cells.[29] Localization of OPN to the nucleus is associated with polo-like kinase-1, a mitosis regulator, in 293 cells.[30]

NF-κB promotes cell survival through enhancing the expression of genes encoding anti-apoptotic proteins, such as Bcl-xL and BFL1 acting at the mitochondria, or IAP1, IAP2, and XIAP, blocking caspase activation.[31,32] Recent data have shown that p50/p65 dimers inhibited *bax* promoter activity, whereas p50/p50 dimers might enhance its activity.[33] Our present study suggests that the proapoptotic function of shOPN may result from, at least in part, impaired NF-κB activation and subsequent inhibition of anti-apoptotic proteins such as Bcl-2/Bcl-xL and XIAP, and an increase of pro-apoptotic protein Bax.

NF-κB is activated in response to several types of chemotherapeutic drugs, which blunts the ability of the cancer therapy to induce cell death.[32] Inhibition of NF-κB activity has been shown as an adjuvant approach to chemotherapy for certain cancers.[32,34] Here, we found that OPN depletion significantly blocked NF-κB activation induced by various chemotherapy drugs in HCC cells. Thus, shOPN might sensitize HCC cells to chemotherapy through inhibition of NF-κB activity. This hypothesis was authenticated by the finding that shOPN promoted chemotherapeutic agents and TRAIL-induced cell death in HCC cells. Importantly, the combination of intratumoral injection of shOPN with systemic administration of 5-FU completely eradicated established human hepatoma in nude mice. Given that HCC is refractory to chemotherapeutic drugs,[23,35] our finding provides a new clue for the treatment of HCC by sensitizing HCC to chemotherapeutic drug–mediated cell death.

In conclusion, our data presented here show that down-regulation of OPN expression in HCC cells significantly inhibits tumorigenesis and metastasis, which might be ascribed to the pro-apoptotic effects induced by OPN depletion. The enhanced sensitivity of HCC cells to chemotherapeutic drugs through blockade of NF-κB activation by OPN silencing may have a great potential in the development of therapeutic regimens for cancer treatment.

References

1. Pan HW, Ou YH, Peng SY, et al. Overexpression of osteopontin is associated with intrahepatic metastasis, early recurrence, and poorer prognosis of surgically resected hepatocellular carcinoma. Cancer 2003;98:119–127.
2. Ye QH, Qin LX, Forgues M, et al. Predicting hepatitis B virus-positive metastatic hepatocellular carcinomas using gene expression profiling and supervised machine learning. Nat Med 2003;9:416–423.
3. Rittling SR, Chambers AF. Role of osteopontin in tumor progression. Br J Cancer 2004;90:1877–1881.
4. Weber GF. The metastasis gene osteopontin: a candidate target for cancer therapy. Biochim Biophys Acta 2001;1552:61–85.
5. Rangaswami H, Bulbule A, Kundu GC. Osteopontin: role in cell signaling and cancer progression. Trends Cell Biol 2006;16:79–87.

6. Khan SA, Lopez-Chua CA, Zhang J, et al. Soluble osteopontin inhibits apoptosis of adherent endothelial cells deprived of growth factors. J Cell Biochem 2002;85:728–736.
7. Geissinger E, Weisser C, Fischer P, et al. Autocrine stimulation by osteopontin contributes to antiapoptotic signalling of melanocytes in dermal collagen. Cancer Res 2002;62:4820–4828.
8. Zohar R, Zhu B, Liu P, et al. Increased cell death in osteopontin-deficient cardiac fibroblasts occurs by a caspase-3-independent pathway. Am J Physiol Heart Circ Physiol 2004;287:1730–1739.
9. Hsieh YH, Juliana MM, Hicks PH, et al. Papilloma development is delayed in osteopontin-null mice: implicating an antiapoptosis role for osteopontin. Cancer Res 2006;66:7119–7127.
10. Lee JL, Wang MJ, Sudhir PR, et al. Osteopontin promotes integrin activation through outside-in and inside-out mechanisms: OPN-CD44V interaction enhances survival in gastrointestinal cancer cells. Cancer Res 2007;67:2089–2097.
11. Wai PY, Mi Z, Guo H, et al. Osteopontin silencing by small interfering RNA suppresses in vitro and in vivo CT26 murine colon adenocarcinoma metastasis. Carcinogenesis 2005;26:741–751.
12. Ito T, Hashimoto Y, Tanaka E, et al. An inducible short-hairpin RNA vector against osteopontin reduces metastatic potential of human esophageal squamous cell carcinoma in vitro and in vivo. Clin Cancer Res 2006;12:1308–1316.
13. Cohen H, Levy RJ, Gao J, et al. Sustained delivery and expression of DNA encapsulated in polymeric nanoparticles. Gene Ther 2000;7:1896–1905.
14. Vasir JK, Labhasetwar V. Polymeric nanoparticles for gene delivery. Expert Opin Drug Deliv 2006;3:325–344.
15. Xu DM, Yao SD, Liu YB, et al. Size-dependent properties of M-PEIs nanogels for gene delivery in cancer cells. Int J Pharm 2007;338:291–296.
16. Xu DM, Hong J, Sheng KL, et al. Preparation of polyethyleneimine nanogels via photo-Fenton reaction. Radiat Phys Chem 2007;76:1606–1611.
17. Bisanz K, Yu J, Edlund M, et al. Targeting ECM-integrin interaction with liposome-encapsulated small interfering RNAs inhibits the growth of human prostate cancer in a bone xenograft imaging model. Mol Ther 2005;12:634–643.
18. Xu G, Nie H, Li N, et al. Role of osteopontin in amplification and perpetuation of rheumatoid synovitis. J Clin Invest 2005;115:1060–1067.
19. Zhao J, Jin J, Zhang X, et al. Transfection of Smac sensitizes tumor cells to etoposide-induced apoptosis and eradicates established human hepatoma in vivo. Cancer Gene Ther 2006;13:420–427.
20. Luan B, Zhang Z, Wu Y, et al. Beta-arrestin2 functions as a phosphorylation-regulated suppressor of UV-induced NF-kappaB activation. EMBO J 2005;24:4237–4246.
21. Ellerbroek SM, Fishman DA, Kearns AS, et al. Ovarian carcinoma regulation of matrix metalloproteinase-2 and membrane type 1 matrix metalloproteinase through beta1 integrin. Cancer Res 1999;59:1635–1641.
22. Mehlen P, Puisieux A. Metastasis: a question of life or death. Nat Rev Cancer 2006;6:449–458.
23. Igney FH, Krammer PH. Death and anti-death: tumour resistance to apoptosis. Nat Rev Cancer 2002;2:277–288.
24. Johnstone RW, Ruefli AA, Lowe SW. Apoptosis: a link between cancer genetics and chemotherapy. Cell 2002;108:153–164.
25. Lin YH, Yang-Yen HF. The osteopontin-CD44 survival signal involves activation of the phosphatidylinositol 3-kinase/Akt signaling pathway. J Biol Chem 2001;276:46024–46030.
26. Scatena M, Almeida M, Chaisson ML, et al. NF-kappaB mediates alphavbeta3 integrin-induced endothelial cell survival. J Cell Biol 1998;141:1083–1093.
27. Guo W, Giancotti FG. Integrin signalling during tumour progression. Nat Rev Mol Cell Biol 2004;5:816–826.
28. Shinohara ML, Lu L, Bu J, et al. Osteopontin expression is essential for interferon-alpha production by plasmacytoid dendritic cells. Nat Immunol 2006;7:498–506.
29. Zohar R, Suzuki N, Suzuki K, et al. Intracellular osteopontin is an integral component of the CD44-ERM complex involved in cell migration. J Cell Physiol 2000;184:118–130.
30. Junaid A, Moon MC, Harding GE, et al. Osteopontin localizes to the nucleus of 293 cells and associates with polo-like kinase-1. Am J Physiol Cell Physiol 2007;292:C919–926.
31. Karin M. Nuclear factor-kappaB in cancer development and progression. Nature 2006;441:431–436.
32. Nakanishi C, Toi M. Nuclear factor-kappaB inhibitors as sensitizers to anticancer drugs. Nat Rev Cancer 2005;5:297–309.
33. Grimm T, Schneider S, Naschberger E, et al. EBV latent membrane protein-1 protects B cells from apoptosis by inhibition of BAX. Blood 2005;105:3263–3269.
34. Wang CY, Cusack JC Jr, Liu R, et al. Control of inducible chemoresistance: enhanced anti-tumor therapy through increased apoptosis by inhibition of NF-kappaB. Nat Med 1999;5:412–417.
35. Johnson PJ. Hepatocellular carcinoma: is current therapy really altering outcome? Gut 2002;51:459–562.

Received September 11, 2007. Accepted May 1, 2008.

Address reprint requests to: Yajun Guo, MD, PhD, International Cancer Institute, Second Military Medical University, 800 Xiang Yin Road, New Building 10-11th Floor, Shanghai 200433, People's Republic of China. e-mail: yjguo@smmu.edu.cn; fax: (86) 21-25074349.

Supported by grants from the National Natural Science Foundation of China, Ministry of Science and Technology of China (973 and 863 project), Shanghai Commission of Science and Technology, a special grant from the E-Institute of Shanghai University's Immunology Division, and the National Foundation for Excellence Doctoral Project.

The authors thank Dr Hongyang Wang for providing the NF-κB–driven luciferase plasmid, and also are grateful to Yunchao Ma, Huaizu Guo, Ling Wang, Qirui Liu, and Yan Huang for technical support.

J.Z. and L.D. contributed equally to this work.